Multimed Tools Appl (2018) 77:6311–6326
DOI 10.1007/s11042-017-4537-9

Thermal comfort research on human CT data modeling

Qingzhen Xu[1] · **Zhoutao Wang**[1] · **Fengyun Wang**[1] · **Jiajia Li**[1]

Received: 9 September 2016 / Revised: 2 February 2017 / Accepted: 20 February 2017 /
Published online: 27 February 2017

Abstract This paper presented a modeling method based on L-W Surface. We obtained our body CT data by CT scan, and get simulation manikin through the 3D reconstruction. We gridded manikin by thermal environment of the digital home, then build multi-scale coupling calculated model based on three-dimensional grid manikins and 25-node physiological model. At last, this paper described the body's adjustment process from the physical point of view, and experimental results showed that the performance of clothing's heat and moisture transfer could be dynamically simulated by computer. It also could get simulation effect of human heat and moisture feeling.

Keywords Heat and moisture exchange · L-W surface · Functional garment CAD

1 Introduction

At the present time, numerical manikins in 3D functional garments CAD has been the focus of research in engineering design and entertainment fields such as high-performance swimwear design. The geometrical configuration, meshing in the pre-treatment and numerical simulation in functional design analysis are necessarily rely on the help of computer science. Based on the surface constructing theory of Bezier, B-Spline and NURBS, Computer Aided Geometric Design (CAGD) played an important role in numerical simulation. The industry already had some commercial platform used to build realistic numerical manikins, such as Poser, Maya, and Rino. However, it had no effective method to produce universal numerical manikins for style design (including 3D virtual stitching) and thermal-moisture comfort analysis in 3D functional garments CAD [1, 4]. Due to different operations has different requirements for numerical manikins, we often need to repair or even re-build the numerical manikins.

✉ Qingzhen Xu
xqz1997@163.com

[1] School of Computer Science, South China Normal University, Guangzhou 510631, China

For example, thermal comfort simulation usually refers to the human body geometry modeling, grid subdivision processing and thermal physiological behaviors regulating. However, there exists geometrical and storage differences in these manikins in different platforms. Hence, universal geometrical modeling methods are needed. Besides, with the development the medicinal technology and the reduce of medical equipment, amount of CT data can be obtained. The CT data with high accuracy and high resolution is helpful for us to understand the distributions of body tissues as well as helpful in human manikin modeling.

A feasible method to solve this problem is to improve the computing speed by parallel computing method. The efficient parallel framework for HEVC proposed by Yan C et al. [14–18] may give you a hint. In this paper, we proposed a new algorithm in a general way which don't need any repair or re-built.

Since rational L-W recurrence surface are generalization of many interpolation or approach parameter surfaces (Bezier, B-Spline, NURBS surface) [8], these surfaces could be used to establish universal storage data file format for different CAD systems, so that the high-speed transmission and conversion of geometric graph of two and three dimension are obtained.

In this paper, our contributions are summarized as follows:

Firstly, we present a 3D dynamic model of heat and moisture transfer. The numerical clothed-manikin is created and meshed by rational L-W recurrence surfaces in multivariate B-form, 25-node and moisture physiology model. We integrate these three models to simulate man's thermal-moisture comfort.

We present a numerical simulation on the heat and moisture exchange between the human body and its surrounding environment. By simulated the heat and moisture transfer from the skin surface to surrounding airflow in the environment, we can generate the 3D dynamic temperature distribution and moisture distribution on the skin surface and in the environment. Figure 1 shows the framework of thermal comfort research in this paper. The rest of this paper is organized as follows. The definition of L-W surface is given in Section 2. The human body manikin geometric model is constructed in Section 3. In Section 4, 25-node thermoregulation model is introduced to describe the thermal regulation behaviors. In Section 5, experiments and discussion are given. Finally, conclusion is drawn.

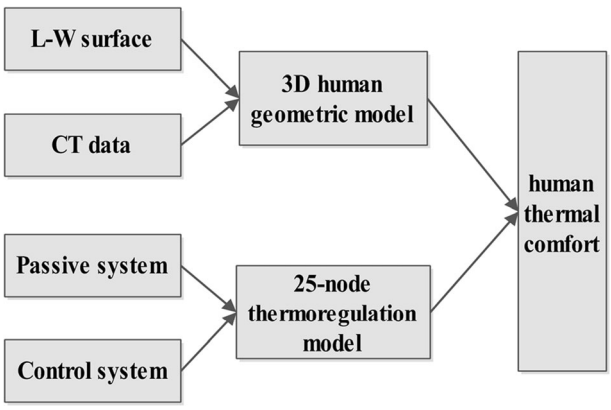

Fig. 1 The framework of thermal comfort research

2 L-W surface definition

L-W recursive surface is first put forward by Luo [8, 9, 12] to construct a general curve surface expression, it takes the general storage file format and form of expression and it can eliminate the conversion error and lower efficiency between surfaces indifferent CAD systems.

In this paper, we give the new form definition of L-surface and W-surface.

Definition 1: Given $(n+1)(m+1)$control vertexes in plane or space$P_{ij}(i=0,1,\ldots,n;$ $j=0,1,\ldots,m)$, We assume $m \geq n$, then

$$R_{i,j}^{k,l}(u,v) = \begin{cases} \left[\lambda_{i,k}(u), \lambda_{i,k}(u)\right] \cdot \begin{bmatrix} R_{i,j}^{k-1,l-1}(u,v) & R_{i,j+1}^{k-1,l-1}(u,v) \\ R_{i+1,j}^{k-1,l-1}(u,v) & R_{i+1,j+1}^{k-1,l-1}(u,v) \end{bmatrix} \cdot \begin{bmatrix} \psi_{j,l}(v) \\ \varphi_{j,l}(v) \end{bmatrix} \\ \text{where } k=1,2,\ldots,n; l=1,2,\ldots,m; \\ i=0,1,\ldots,n-k; j=0,1,\ldots,m-1 \\ P_{i,j} \qquad \text{where } k=0, l=0; i=0,1,\ldots,m \end{cases} \tag{1}$$

where $u \in [a,b]$, $v \in [a,b]$

The surface $R_{0,0}^{n,m}(u,v)$is called the $n \times mth$ rational L-surface, abbreviated as$R(u,v)$.

Where

$$\lambda_{i,k}(u) = \frac{(\gamma\beta_k + 1)(u + \alpha_l)}{(\alpha_i + \beta_k)(\gamma u + 1)}$$

$$\mu_{i,k}(u) = \frac{(1-\gamma\alpha_i)(\beta_k - u)}{(\alpha_i + \beta_k)(\gamma u + 1)}$$

$$\psi_{j,l}(v) = \frac{(hd_l + 1)(v + c_j)}{(c_j + d_l)(hv + 1)}$$

$$\varphi_{j,l}(v) = \frac{(1-hc_j)(d_l - v)}{(c_j + d_l)(hv + 1)}$$

Notice the coefficients.

$\gamma, \alpha_i, \beta_k, h, c_j, d_l(i=0,1,\ldots,n; k=0,1,\ldots,n; j=0,1,\ldots,m; l=0,1,\ldots,m)$,

Obviously,

$$\lambda_{i,k}(u) + \mu_{i,k}(u) = \frac{(\gamma\beta_k + 1)(u + \alpha_i)}{(\alpha_i + \beta_k)(\gamma u + 1)} + \frac{(1-\gamma\alpha_i)(\beta_k - u)}{(\alpha_i + \beta_k)(\gamma u + 1)} = 1$$

$$\psi_{j,l}(v) + \varphi_{j,l}(v) = \frac{(hd_l + 1)(v + c_j)}{(c_j + d_l)(hv + 1)} + \frac{(1-hc_j)(d_l - v)}{(c_j + d_l)(hv + 1)} = 1$$

If $0 \leq \lambda_{i,k}(u), \mu_{i,k}(u), \psi_{j,l}(v), \varphi_{j,l}(v) \leq 1$, the surface $R_{0,0}^{n,m}(u,v)$is called then$\times mth$ rational W-surface, abbreviated as$W(u,v)$.

Suppose $R_{0,0}^{n,m}(u,v)$ is the $n \times mth$ rational L-surface, if $\gamma = 0, h = 0, R_{0,0}^{n,m}(u,v)$is called the standard $n \times mth$ rational L-surface, that is to say L-surface.

Now

$$R_{i,j}^{k,l}(u,v) = \begin{cases} \left[\lambda_{i,k}(u), \lambda_{i,k}(u)\right] \cdot \begin{bmatrix} R_{i,j}^{k-1,l-1}(u,v) & R_{i,j+1}^{k-1,l-1}(u,v) \\ R_{i+1,j}^{k-1,l-1}(u,v) & R_{i+1,j+1}^{k-1,l-1}(u,v) \end{bmatrix} \cdot \begin{bmatrix} \psi_{j,l}(v) \\ \varphi_{j,l}(v) \end{bmatrix} \\ \text{where} \quad k = 1,2,\ldots,n; l = 1,2,\ldots,m; \\ i = 0,1,\ldots,n-k; j = 0,1,\ldots,m-l \\ P_{i,j} \quad k = 0, l = 0; i = 0,1,\ldots,m \end{cases} \tag{2}$$

where

$\lambda_{i,k}(u) = \frac{(u+\alpha_i)}{} (\alpha_i + \beta_k)$ $\mu_{i,k}(u) = \frac{(\beta_k - u)}{} (\alpha_i + \beta_k)$

$\psi_{j,l}(v) = \frac{(v+c_j)}{} (c_j + d_l)$ $\varphi_{j,l}(v) = \frac{(d_l - v)}{} (c_j + d_l)$

Definition 2: Transform from Bezier surface to L-Surface and W-Surface. The recurrence form of Bezier surface can be shown as follows.

$$V_{i,j}^{k,l}(u,v) = \begin{cases} [1-u, u] \cdot \begin{bmatrix} V_{i,j}^{k-1,l-1}(u,v) & V_{i,j+1}^{k-1,l-1}(u,v) \\ V_{i+1,j}^{k-1,l-1}(u,v) & V_{i+1,j+1}^{k-1,l-1}(u,v) \end{bmatrix} \cdot \begin{bmatrix} 1-v \\ v \end{bmatrix} \\ \text{where} \quad k = 1,2,\ldots,n; l = 1,2,\ldots,m; \\ i = 0,1,\ldots,n-k; j = 0,1,\ldots,m-l \\ P_{i,j} \quad k = 0, l = 0; i = 0,1,\ldots,m \end{cases} \tag{3}$$

$$u \in [0,1], v \in [0,1]$$

Let $\gamma = 0$, $\alpha_i = -1$, $\beta_k = 0$, $h = 0$, $c_j = -1$, $d_l = 0$

$$(i = 0,1,\ldots,n; k = 0,1,\ldots,n; k = 0,1,\ldots,m; l = 0,1,\ldots,m)$$

Then $\lambda_{i,k}(u) = 1 - u$, $\mu_{i,k}(u) = u$, $\psi_{j,l}(v) = 1 - v$; $\varphi_{j,l}(v) = v$.

Obviously,$G_{0,0}^{n,m}(u,v) = V_{0,0}^{n,m}(u,v)$, therefore Bezier surface is a standard L-surface.

As$u \in [0,1]$, $v \in [0,1]$, $0 \le \lambda_{i,k}(u)$, $\mu_{i,k}(u)$, $\psi_{j,l}(v)$, $\varphi_{j,l}(v) \le 1$, therefore Bezier surface is also a standard W-surface.

Definition 3:Transform from discrete B-spline surface to L-surface. Given $(n+1)(m+1)$control vertices $P_{i,j}(i = 0, 1, \ldots, n; j = 0, 1, \ldots, m)$in the space or plane, arbitrary fixed parameter $u \in [u_r, u_{r+1}]$, $v \in [v_p, v_{p+1}]$; $s \le r \le n$, $q \le p \le m$.

The $r \times p$section of $n \times qth$ discrete B-spline surface can be recurrently shown as follows:

$$R_{i,j}^{k,l}(u,v) = \begin{cases} \left[\frac{u-u_i}{u_{i+r-k}-u_i}, \frac{u_{i+r-k}-u}{u_{i+r-k}-u_i}\right] \cdot \begin{bmatrix} V_{i,j}^{k-1,l-1}(u,v) & V_{i,j+1}^{k-1,l-1}(u,v) \\ V_{i+1,j}^{k-1,l-1}(u,v) & V_{i+1,j+1}^{k-1,l-1}(u,v) \end{bmatrix} \cdot \begin{bmatrix} \frac{v-v_j}{v_{j+p-q}-v_j} \\ \frac{v_{j+p-q}-v}{v_{j+p-q}-v_j} \end{bmatrix} \\ \text{where} \quad k = 1,2,\ldots,r-1; l = 1,2,\ldots,p-1; \\ i = r-s-1,\ldots,2r-s-k-2; j = p-q-1,\ldots,2p-q-l-2 \\ P_{i,j} \quad k = 0, l = 0; i = s-r+1, s-r+2,\ldots,s; \\ j = q-p+1, q-p+2,\ldots,q; \end{cases} \tag{4}$$

We made subscripts transformation on definition 1 as follows:

$\{ i = i + (s-r+1)\ \ n = r-1\ \{ j = j + (q-p+1)\ \ m = p-1$

Furthermore, let $\gamma = 0$, $\partial_i = -u_i$, $\beta_k = u_{i+r-k}$, $h = 0$, $c_j = -v$, $d_l = v_{i+p-q}$.

Obviously$G_{0,0}^{n,m}(u,v) = R_{0,0}^{n,m}(u,v)$, therefore discrete B-spline surface section is also a standard L-Surface.

Surface representation is closely related to the choice of parameter region. If the rectangular parameter region is selected, the tensor product or Boolean form is usually used to construct the surface. If the triangle region is chosen, the direct-order construction method is adopted.

Definition 4: Set $\left\{d_\alpha \middle| |\alpha| = n, \alpha \in Z_+^3\right\}$ as the vertex of the characteristic network on the triangle domain.

$$\begin{cases} d_\alpha^0 = d_\alpha \qquad \left|\alpha\right| = n, \\ d_\alpha^r(u,v,w) = L_\alpha^r(u) d_{\alpha+J_0}^{r-1}(u,v,w) + M_\alpha^r(v) d_{\alpha+J_1}^{r-1}(u,v,w) + N_\alpha^r(w) d_{\alpha+J_2}^{r-1}(u,v,w), \\ L_\alpha^r(u) + M_\alpha^r(v) + N_\alpha^r(w) = 1; r = 1,2,\ldots,n; \left|\alpha\right| = n-r. \end{cases} \tag{5}$$

This is define as a n steps recursive surface in the triangular domain. And $L_\alpha^r(u) + M_\alpha^r(v) + N_\alpha^r(w) \equiv 1; r = 1,2,\ldots,n; |\alpha| = n-r$. If the component α in $L_\alpha^r(u), M_\alpha^r(v), N_\alpha^r(w)$ $(r = 1,2,\ldots,n)$is less than 0,$L_\alpha^r(u) = 0, M_\alpha^r(v) = 0, N_\alpha^r(w) = 0$.

If

$L_\alpha^r(u) = a_\alpha^r u + b_\alpha^r, M_\alpha^r(v) = c_\alpha^r v + d_\alpha^r, L_\alpha^r(u) = N_\alpha^r(w) = e_\alpha^r w + f_\alpha^r = 1 - L_\alpha^r(u) - M_\alpha^r(v)$ the $d_\alpha^n(u,v,w)$ $(|\alpha| = 0)$is called as n sub recursive surface.

Definition 5: N sub recursive surfaces in the triangular domain $d_\alpha^n(u,v,w)$ $(|\alpha| = 0)$,if $L_\alpha^r(u)$, $M_\alpha^r(w), N_\alpha^r(v)$ coefficient $a_\alpha^r, b_\alpha^r, c_\alpha^r, d_\alpha^r$ can satisfies the situation that cam be shown as follows.

$$\begin{cases} a_{\alpha+J_0}^r b_\alpha^{r+1} = b_{\alpha+J_0}^r a_\alpha^{r+1}, a_{\alpha+J_1}^r b_\alpha^{r+1} = b_{\alpha+J_1}^r a_\alpha^{r+1}, \\ c_{\alpha+J_1}^r d_\alpha^{r+1} = d_{\alpha+J_1}^r c_\alpha^{r+1}, c_{\alpha+J_2}^r d_\alpha^{r+1} = d_{\alpha+J_2}^r c_\alpha^{r+1}, \\ a_{\alpha+J_2}^r \left(1 - b_\alpha^{r+1} - d_\alpha^{r+1}\right) = a_\alpha^{r+1}\left(1 - b_{\alpha+J_2}^r - d_{\alpha+J_2}^r\right), \\ c_{\alpha+J_2}^r \left(1 - b_\alpha^{r+1} - d_\alpha^{r+1}\right) = c_\alpha^{r+1}\left(1 - b_{\alpha+J_2}^r - d_{\alpha+J_2}^r\right), \\ a_{\alpha+J_0}^r \left(1 - b_\alpha^{r+1} - d_\alpha^{r+1}\right) = a_\alpha^{r+1}\left(1 - b_{\alpha+J_0}^r - d_{\alpha+J_0}^r\right), \\ c_{\alpha+J_0}^r \left(1 - b_\alpha^{r+1} - d_\alpha^{r+1}\right) = c_\alpha^{r+1}\left(1 - b_{\alpha+J_0}^r - d_{\alpha+J_0}^r\right), \end{cases} \tag{6}$$

Where $a_\alpha^{r+1}, c_\alpha^{r+1}, a_{\alpha+J_i}^r, c_{\alpha+J_i}^r \neq 0 (i = 0,1,2)$,the surface $d_\alpha^n(u,v,w)$ $(|\alpha| = 0)$is called triangular domain rational L-surface.

If $0 \le L_\alpha^r(u), M_\alpha^r(w), N_\alpha^r \le 1$,the gotten surface $d_\alpha^n(u,v,w)$ $(|\alpha| = 0)$ is called the triangular domain rational W-surface.

Definition 6: Transform from Bezier surface to L-surface in the triangular domain. Now we take the recursive form of the three B-B surface as an example. Three B-B surfaces of recursive form can be shown as follows.

$$\begin{cases} d_\alpha^0(u,v,w) = d_\alpha \qquad \left|\alpha\right| = 3, \\ d_\alpha^r(u,v,w) = u d_{\alpha+J_0}^{r-1}(u,v,w) + v d_{\alpha+J_1}^{r-1}(u,v,w) + w d_{\alpha+J_2}^{r-1}(u,v,w), \\ u+v+w = 1; r = 1,2,3; \left|\alpha\right| = n-r. \end{cases} \tag{7}$$

As long as given $L_0^n, M_{0,}^n N_0^n$ and $K_{j,0,0}^r, G_{0,j,0}^r, I_{0,0,j}^r$,.

$k_{0,j,0}^r, g_{0,0,j}^r, i_{j,0,0}^r; j = n-r, r = 2,3,\ldots,n$;we can determine the $L_\alpha^r, M_\alpha^r, N_\alpha^r (|\alpha| = n-r)$. Let $L_\alpha^r = u, M_\alpha^r = v, N_\alpha^r = w (|\alpha| = 3-r, r = 1,2,3)$.That is $L_{0,0,0}^3 = u, M_{0,0,0}^3 = v, N_{0,0,0}^3 = w, u+v+w = 1$and $K_{j,0,0}^r = k_{0,j,0}^r = G_{0,j,0}^r = g_{0,0,j}^r = I_{0,0,j}^r = i_{i,0,0}^r = 1; r = 2,3; j = 3-r$.

Therefore Three B-B surfaces of recursive form is a L-surface, so we could know Bezier surface is also a L-surface in the triangular domain.

The above is the mathematical modeling method, and the experiment data obtained through the 256-slice CT scan. We use the new algorithm proposed by us to carry out three-dimensional reconstruction, getting a numerical manikins, and everyone's CT data could be directly converted into a 3D reconstruction model.

The construction and grid of the numerical CT data is the most common physiological data and it is helpful for us to understand the human body constitutes as well as tissue distributions. On basis of the geometric definition of L-surface and W-surface and the collected CT data, we construct a compact human body model which aims to used in human thermal comfort evaluation.

Instead of using a human body model, which is uniform material, teapot-like closed surface in the CTM model proposed by Murakamis et al. [10], we use the NURBS curve model to generate the outline contour of the human body and then generate the human body shape surface. The geometric model is generated by the contour surface of the human body and then divided to form the files we need. In this way, we realized a transformation from the CTM model to a numerical manikin. The specific implementation steps are as follows:

1) Carry out CT scans on human body, and classify the scanned CT data according to the height value of each body points. so as to build the topological geometry relationship between the deformation data.
2) Filter the CT data which significant influence on the shape of human body and take use of definition of L-surface and W-surface to construct human body model. The human body shape surface can be shown in Fig. 2.
3) Generate the human body shape surface and solid simulation model, shown in Fig. 3 and Fig. 4.
4) Mesh on the human body and the surrounding environment. The triangle mesh subdivision technology combined with quadrilateral mesh subdivision method are used and the meshed model is shown in Fig. 5.

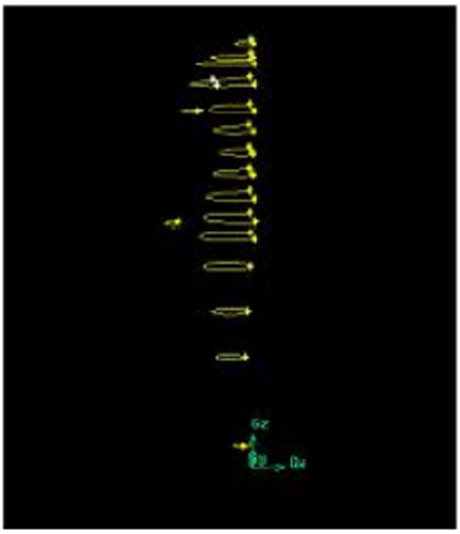

Fig. 2 Human body contour line(half body)

As the workload of "input patch" method for modeling is very large, and the loss of data points is much more, it could not be able to constitute an ideal volume for calculation grid. So we used the method from bottom to top, using the geometric modeling method to build the human body model. We input the horizontal scanning coordinates of data point of human body through the layers of data points to the surface of the human body, and generate the closed contour surface geometry as shown in Fig. 2 and Fig. 3.

Due to the irregular curvature distribution of the geometrical model of the human body, it is difficult to grid the human model with the same standard. While the size of grid was too large, it would inevitably result in the low efficiency and low accuracy during numerical simulation. Hence, a moderate intermediate is given to obtain the distribution of the grid, a variety of

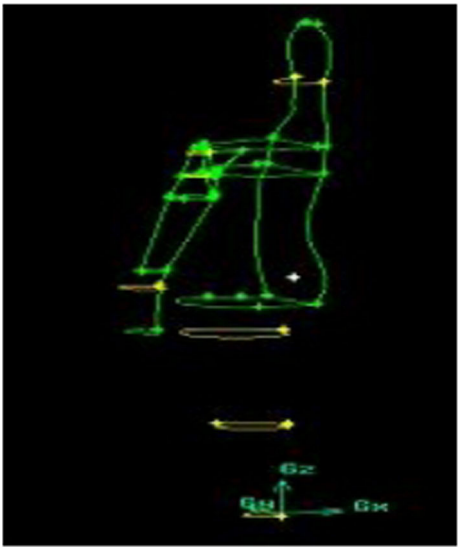

Fig. 3 Human body contour surface

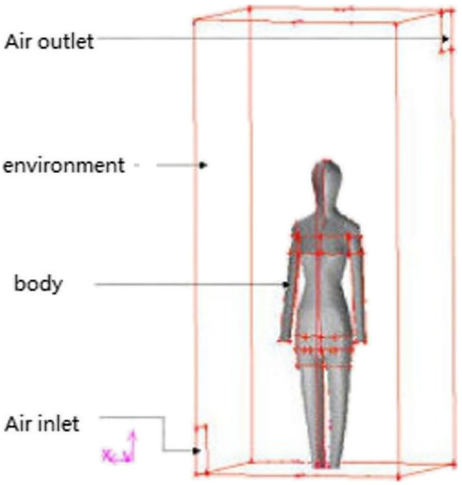

Fig. 4 The geometric model of the human body and the surrounding environment

standard grid divisions are adopted to find a suitable match to relieve the contradiction of the computation and accuracy [11].

The numerical manikin can not be distorted, and looks like a human body. This paper is the study of human cognition and exchange under the dress form. Therefore, it is necessary to have dress numerical human body model, and to ensure that the structure of the human body model can be carried out in the grid, the grid is prerequisite for numerical analysis.

In order to carry out thermal comfort research, we have to set up a geometric model of the human body and the surrounding environment in the digital home environment, as shown in

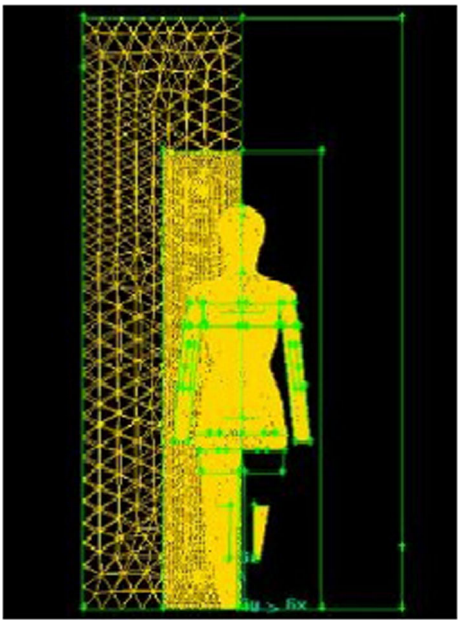

Fig. 5 Human body surrounding environment after split

Fig. 4. The environment relates to the human body, clothing, body-clothing microenvironment and the surrounding environment with large scale difference in the thickness and the curvature, there is no effective meshable dominant human body-clothing-environment geometry yet. Therefore, the grid of human-body environment model shown in Fig. 5 was produced by the Gambit, for the sake of clarity, we only gave a part of the grid, and take the impact of clothing into account of the following analysis module.

Due to the complexity of the geometrical model of the human body, which has irregular curvature distribution, it is difficult to use the same standards to the grid. If the size of grid was too large, it would inevitably result in the low efficiency of numerical simulation; otherwise, the accuracy would be reduced and could not reflect the simulation well. In Fig. 5, joined a moderate intermediate to obtain the distribution of the grid, using a variety of standard grid division as step 4 has mentioned, it could relieve the contradiction of the computation and accuracy [11], but we need to find a suitable match.

3 Human thermoregulation model

The human thermoregulation mechanisms directly affects the thermal status and the thermal comfort can be evaluated on the basis of the thermal status especially the temperature and sweat distributions of body.

25-node thermoregulation model has become the standard of anatomy method to simulate the human thermal regulation mechanisms [7, 19]. It is applied in our work to study the thermal behaviors under various circumstances. 25-node model is usually modeled from two aspects: passive system and control system. Passive system describes the person's own mathematics geometric model and heat transfer model. Control system describes the temperature regulating mechanisms such as sweating, trembling, change of heat flow, etc. The mathematical models are given as follows.

Passive system:

$$\begin{aligned} C_{p,n}\frac{dT_n}{dt} &= M_n - B_n - K_n - R_n - C_n - (E_n + E_{res}), \\ & \qquad n = 1, \ldots, 24; p = 1, 2, 3, 4 \\ C_b\frac{dT_b}{dt} &= \sum_{n=1}^{24} B_n \end{aligned} \tag{8}$$

Control system:

$$e_n = T_n - T_{n,set}$$

where, Cp,n and Cb are the thermal capacity of body points and central blood, Mn is the metabolic heat production, Bn is thermal exchange between body nodes and central blood, Kn is the heat loss by work, Rn is the heat loss by radiation, Cn is the heat loss by conduction, En is the heat loss by evaporation, and Eres is the heat loss by respiration. en is the error signal of thermoregulation system. Tn is the current temperature, Tn,set is the threshold of the human body.

From this mathematical model, a large number of human physiological vitals can be simulated. According to these simulation results, we evaluate the human thermal comfort by the reference of Du [13] and Jia [5].

4 Numerical analysis results

The calculation models used in this paper were $k-\varepsilon$ model to simulate the air turbulent environment, diffusion model that mimics the mixture of water vapor exchange system, and Gagge 24-node model to simulate the human body's own thermal physiological regulation [7, 19]. The user defined function (UDF) would be three models in the human body-environment of the contact boundary interface. At present, the analysis on the heat and moisture exchange numerical simulation model of the human body-environment, with no explicit consideration of the geometry of the clothing, just relied on the use of the physical model of clothing thermal resistance parameters [2, 3, 6]. This kind of consideration could not simulate the dynamic heat and moisture exchange phenomenon in the dressed state. How to construct the dressed human body model was a difficult problem in the analysis of heat and moisture. There were two possible solutions to the problem of clothing, one was the geometric model of the dominant structure clothes, the other was the model of the hidden structure clothes. The hidden structure of the clothing was reflected in the definition of the inner and outer surface layer of manikin with different material properties, specifically, the outer surface was defined as garment property and the inner one as the skin. In this way, we defined and introduced the clothed-manikin.

In this section, we show some visualization results of the body temperature and humidity distributions. Assume that people with 1.651 m, 65.5 kg stands in a ventilation room, the room temperature is 303 k, the relative humidity is 9.5 g/kg, and the wind velocity is 0.12 m/s. We simulate the thermal status by computer.

4.1 Simulation result

Body surface temperature is distributed in [303.34, 303.345]. As shown in Fig. 6, the body surface temperatures are distributed unevenly, red yellow and green are more, and the blue was less. The temperature of red was mainly in [303.3446, 303.34464], the temperature of yellow was mainly in [303.34363, 303.34369], the temperature of green is mainly in [303.34277, 303.3428], and the temperature of blue was mainly in [303.34186, 303.34189].

The environment temperature is distributed in [301.50, 302.07]. As we can see from the Fig. 7, the surrounding environment of the body is mainly composed by red/pale red/brown, the edge of the environment is composed by yellow/green/blue. The red areas represent the temperature in [302.013, 302.0415], the pale red areas represent the temperature in [301.9845, 302.013], the brown areas represent the temperature in [301.95599, 301.9845], the yellow areas represent the temperature in [301.87051, 301.89902], the green areas represent the temperature in [301.84201, 301.87051], the blue areas represent the temperature in [301.5284, 301.55701].

Humidity on the surface of the body is mainly distributed in [0.817433, 0.817490], due to the effective number of reasons fail to show in Fig. 8. As we can see from Fig. 8, it is mainly composed of distribution of red yellow, green and blue. Red is distributed in the body, the moisture of red is mainly within [0.81748402, 0.81748402], the moisture of yellow is mainly in [0.81747502, 0.81747502], the moisture of green is mainly in [0.81746, 0.81746101], the moisture of blue is mainly in [0.81744403, 0.81744498].

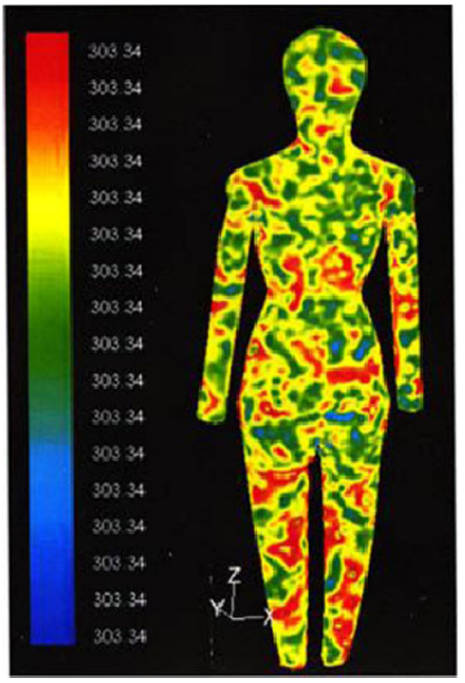

Fig. 6 The temperature distribution on the surface of the human body

The humidity of environment is mainly distributed in [0.60, 0.72]. As shown in Fig. 9, the distribution of the environmental moisture is not uniform and the level is

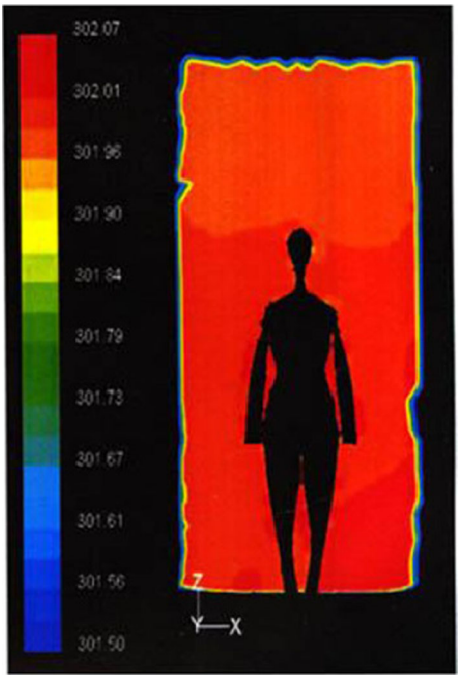

Fig. 7 The temperature distribution of the environment

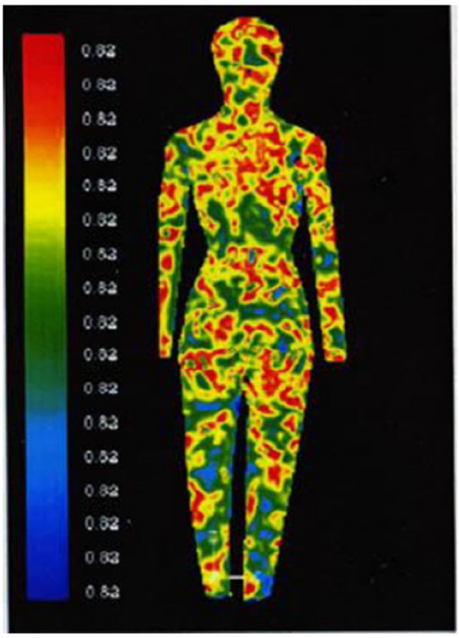

Fig. 8 Moisture distribution on the surface of the body

clear, the lower left corner of the air inlet has the lowest moisture, that is, the sky blue in Fig. 9. From the outside to the inside of the moisture are respectively in [0.61199999, 0.61799997], [0.91799997, 0.62400001], [0.62400001, 0.63], [0.63,

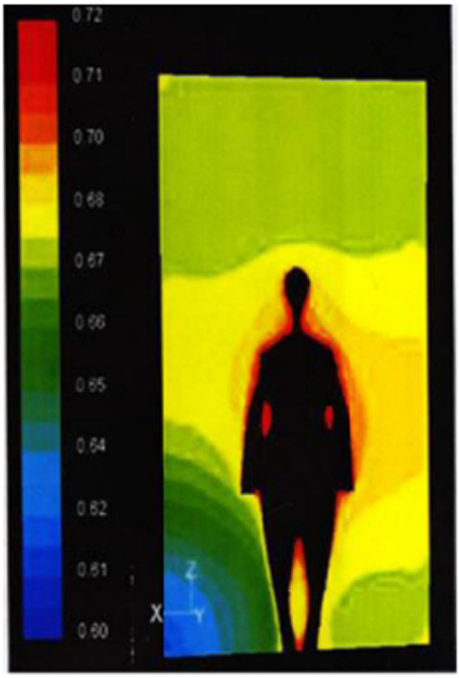

Fig. 9 Moisture distribution of the environment

0.63599998]. The lower left of the green area of the moisture is distributed in [0.618,0.65399998], the lower right corner of the shallow green area of moisture is distributed in the [0.6719999,0.67799997], the lower right corner of the yellow area of moisture is distributed in the [0.67799997,0.68400002], the yellow area of the top of the head is distributed in [0.67799997,0.68400002], the light blue area of the top of the head is distributed in [0.67199999,0.67799997], the red area of the body surface is distributed in [0.708,0.71399999], the brown area near the body is distributed in [0.69,0.69599998] and the brown area of the moisture is distributed in [0.68400002,0.69].

The moisture of body surface is mainly distributed in [0: 817433; 0: 817490] which fail to show in Fig. 8 due to the limit of significant digits. In Fig. 8, it is mainly composed of red, yellow, green and blue, the red is distributed throughout the body. Where the red represents the moisture is mainly within [0.81748402, 0.81748402], the yellow for [0.81747502, 0.81747502], the green for [0.81746, 0.81746101], the blue for [0.81744403, 0.81744498].

The moisture of environment is mainly distributed in [0.60, 0.72]. In the Fig. 9, the distribution of the environmental moisture is not uniform and the level of color is clear, the air inlet, the area of azure color in bottom left corner of the Fig. 9, had the lowest moisture. In the following, we'll explain the moisture distribution in detail. In the bottom left corner, the moisture of the azure area is respectively within [0.61199999, 0.61799997], [0.61799997, 0.62400001], [0.62400001, 0.63], [0.63, 0.63599998] from the outside to the inside, the green area is within [0.618, 0.65399998]. In the bottom right corner, the moisture of shallow green area within [0.6719999, 0.67799997], the yellow area is [0.67799997, 0.68400002]. In the top, the yellow area is [0.67799997, 0.68400002] and the light blue area is [0.67199999, 0.67799997]. In the body part, the red contour of the manikin is [0.708, 0.71399999], the brown area nearby is [0.69, 0.69599998] and the light brown area is [0.68400002, 0.69].

4.2 Discussion

The CTM model suggests that the complex physical shape of the human body influences the heat and moisture exchange of the body and the environment, and the temperature distribution of the body surface and environment is not uniform. Just as shown in the above figures. The temperature of body surface is distributed in [303.341, 303.345], higher than the initial skin temperature which is 303 K, indicating that the human skin is endothermic in the heat exchange process. While the environmental temperature, with the initial temperature of 303 K, distribution in [301.50, 302.07], indicating that the environment in the heat exchange process loss of heat.

From the Fig. 6 and Fig. 7 we could know that the temperature exchange of manikin and environment is not obviously.

In Fig. 8 and Fig. 9, the moisture distribution of environment and body surface is uneven. The initial absolute moisture of body surface is 0, while after simulation, it's mainly distributed in [0.817433, 0.817490], this shows that the skin with adsorption. While the environment moisture is mainly distributed in [0.60, 0.72], this shows that the moisture spread, a part of the moisture was taken away, resulting in the body surface moisture higher than the body's surrounding environment.

5 Conclusion

In this paper, we establish a new three-dimensional human body meshed parametric model based on L-W surface and the CT data which considers the body heat regulating system and environmental Multiple factors to do thermal comfort simulation. The new model could simulate heat and moisture exchange process between human body and environment. The main features are simplified and efficient three-dimensional model. It could better reflect the good simulation process. Although the process described in this chapter is feasible, and its performance is directly influenced by the geometry of the numerical model of the human body. For example, the number of hidden grid construction and garment geometric model directly affects the numerical simulation of the efficiency and accuracy. The universal values of human manikin directly impact on the further development of three-dimensional functional clothing CAD. The relevant difficulties in this field also need to be further in-depth study. It'll be researched in the future paper.

Acknowledgements The Project was supported by the National Natural Science Foundation of China (No.61402185), Natural Science Foundation of Guangdong Province (No. 2015A030313382), and Guangdong Provincial Public Research and Capacity Building Foundation funded project (Nos. 2016A020223012).

References

1. Cheng Y, Niu J, Gao N (2012) Thermal comfort models: a review and numerical investigation. Build Environ 47:13–22
2. Havenith G, Heus R, Lotens WA (1990a) Resultant clothing insulation—a function of body movement, posture, wind, clothing fit and ensemble thickness[J]. Ergonomics 33(1):67–84
3. Havenith G, Heus R, Lotens WA (1990b) Clothing ventilation, vapor resistance and permeability index_changes due to posture, movement and wind[J]. Ergonomics 33(8):989–1005
4. R. Holopainen (2012) A human thermal model for improved thermal comfort, Ph. D. Thesis, Aalto University
5. Jia N, Yu L, Yang KX et al (2016) A novel exercise Thermophysiology comfort prediction model with fuzzy logic[J]. Mob Inf Syst. doi:10.1155/2016/8586493
6. Li Y, Wang Z, Hu J Y (1999) Mathematical simulation and experimental verification of fabric thermal and moisture perceptions‖the SEM Annual Conference on The Interdependence Between Theoretical, Experimental and Computational Mechanics[C].Cincinnati, USA
7. Li Y, QY Zhu, and ZX Luo (2001) Numerical simulation of heat transfer coupled with moisture sorption and liquid transport in porous textiles. In the 6th Asian Textile Conference. Hong Kong
8. Luo X, Nie H et al (2002) Recurrence surfaces on arbitrary quadrilateral mesh. J Comput Appl Math 144: 221–232
9. Luo XN, Liu N, Gao CY (2004) Fairing geometric modeling based on 4-point interpolatory subdivision scheme. J Comput Appl Math 163(1):189–197
10. Murakami S, Kato S, Zeng J (1998) Combined simulation of airflow, radiation and moisture transport for heat release from human body[J]. Roomvent 98(b):141–150
11. Shin-ichi Tanabe, Kozo Kobayashi, Junta Nakano, Yoshiichi Ozeki (2002) Evaluation of Thermal comfort using combined multi-node termoregulation (65MN) and radiation models and computational fluid dynamics (CFD), Energy and Buildings 34(6):637–646
12. Wang R, Li Y et al (2004) Rational recurrence curves and recurrence surfaces in multivariate B-form on some regions. J Comput Appl Math 163:277–285
13. Wang R, Du H, Zhou F, Deng D, Liu Y (2014) An adaptive neural fuzzy network clothing comfort evaluation model and application in digital home. Multimedia Tools and Applications 71:395–410

14. Yan C, Zhang Y, Dai F et al (2013) Highly parallel framework for HEVC motion estimation on many-Core platform[C]// data compression conference. IEEE Computer Society 63-72
15. Yan C, Zhang Y, Xu J et al (2014a) A highly parallel framework for HEVC coding unit partitioning tree decision on many-core processors[J]. IEEE Signal Processing Lett 21(5):573–576
16. Yan C, Zhang Y, Xu J et al (2014b) Efficient parallel framework for HEVC motion estimation on many-Core processors[J]. IEEE Trans Circuits Syst Video Technol 24(12):2077–2089
17. Yan C, Zhang Y, Dai F et al (2014c) Parallel deblocking filter for HEVC on many-core processor[J]. Electron Lett 50(5):367–368
18. Yan C, Zhang Y, Dai F et al (2014d) Efficient parallel HEVC intra-prediction on many-core processor[J]. Electron Lett 50(11):805–806
19. Zhu F, Yu Z, Qianqian F, Dehong X (2013) Moisture diffusivity in structure of random fractal fiber bed. Physics Letter A 377:2324–2328

Qingzhen Xu received his PhD in computer science from SUN YAT-SEN UNIVERSITY in the years 2006. He is presently serving as a professor in school of computer science at South China Normal University.

Zhoutao Wang is a graduate student of computer science at South China Normal University. In the study period, he has excellent grades. His research interests include machine learning, digital image processing. He participated in the Natural Science Foundation of Guangdong Province and so on.

Fengyun Wang is a graduate student of computer science at South China Normal University, majoring in software engineering, she research interests mainly include digital image processing. She participated in the Natural Science Foundation of Guangdong Province and so on.

Jiajia Li is a graduate student of computer science at South China Normal University. In the study period, she has excellent grades, and she won the scholarship every year. During the graduate school, she participated in the National Natural Science Foundation of China, Natural Science Foundation of Guangdong Province, and Guangdong Provincial Public Research and Capacity Building Foundation funded project and so on.